Published in "Langmuir 26(19): 15634–15643, 2010"
which should be cited to refer to this work.

Structure and "Surfactochromic" Properties of Conjugated Polyelectrolyte (CPE): Surfactant Complexes between a Cationic Polythiophene and SDS in Water

Matti Knaapila,*[,†] Rachel C. Evans,[‡] Vasil M. Garamus,[§] László Almásy,[⊥,#] Noémi K. Székely,[∥] Andrea Gutacker,[▽] Ullrich Scherf,[▽] and Hugh D. Burrows[○]

[†]*Physics Department, Institute for Energy Technology, NO-2027 Kjeller, Norway,* [‡]*School of Chemistry, Trinity College Dublin, Dublin 2, Ireland,* [§]*GKSS Research Centre, D-21502 Geesthacht, Germany,* [⊥]*Laboratory for Neutron Scattering, PSI, CH-5232 Villigen, Switzerland,* [#]*Adolphe Merkle Institut, University of Fribourg, CH-1700 Fribourg, Switzerland,* [∥]*Research Institute for Solid State Physics and Optics, Budapest-1525, Hungary,* [▽]*Fachbereich Chemie, Bergische Universität Wuppertal, D-42097 Wuppertal, Germany, and* [○]*Departamento de Química, Universidade de Coimbra, 3004-535 Coimbra, Portugal*

We report on the phase transitions, solution structure, and consequent effect on the photophysical properties of poly[3-(6-trimethylammoniumhexyl)thiophene] bromide (P3TMAHT) in aqueous sodium dodecylsulfate (SDS). Polythiophene was mixed with SDS or deuterated SDS to form P3TMAHT(SDS)$_x$ complex (x = the molar ratio of surfactant over monomer units) in D_2O and studied by small-angle neutron and X-ray scattering (SANS/SAXS) and optical spectroscopy. At room temperature, P3TMAHT forms charged aggregates with interparticle order. The addition of SDS eliminates the interparticle order and leads to rod-like (x = 1/5) or sheet-like polymer−SDS aggregates (x = 1/2 to 1) containing rod-like (x = 1/5 to 1/2) or sheet-like (x = 1/2 to 1) polymer associations. Partial precipitation occurs at the charge compensation point (x = 1). Ellipsoidal particles without interparticle order, reminiscent of SDS micelles modified by separated polymer chains, occur for x = 2 to 5. Free SDS micelles dominate for x = 20. Structural transitions lead to a concomitant variation in the solution color from red (P3TMAHT) to violet (x = 1/5 to 1) to yellow (x > 2). The photoluminescence fingerprint changes progressively from a broad featureless band (x = 0) through the band narrowing and appearance of vibronic structure (x = 1/5 to 1) to the return to a blue-shifted broad emission band (x = 5). The polymer stiffness reaches a maximum for x = 1, which leads to minimization of the Stokes shift (0.08 eV). This work gives fundamental information upon how surfactant complexation can influence both the solution structure and photophysical properties of a water-soluble polythiophene.

Introduction

Since the introduction of water-soluble π-conjugated polymers in the 1980s,[1] they have been developed for diverse applications including light emitting diodes,[2] chemosensors,[3] and biosensors,[4] where water provides a non-noxious media for device environment or signal amplification. Control of the water−polymer interaction is desirable for polymer deposition in inkjet,[5] layer-by-layer,[6,7] and Langmuir−Blodgett[8] processes. Strategies to control solubility in water include incorporation of hydrophilic terminal groups such as noncharged ethynylene[9] or charged amino groups[10] into side chains off the polymer backbone. Sophisticated π-conjugated polyelectrolytes[11] and charge-transfer supramolecules[12] have been introduced in water. Another possibility is the combination of two ionomers as with the well-known example of poly(3,4-ethylenedioxythiophene) and poly(4-styrenesulfonate).[13] In another strategy, water solubility is controlled by nonionic[14] or ionic[15] surfactants that may form a layer between the polymer and

*Corresponding author. Tel: +47-6380-6081. Fax: +47-6381-0920. E-mail: matti.knaapila@ife.no.

(1) Patil, A. O.; Ikenoue, Y.; Wudl, F.; Heeger, A. J. *J. Am. Chem. Soc.* **1987**, *109*, 1858–1859.

(2) (a) Hoven, C. V.; Garcia, A.; Bazan, G. C.; Nguyen, T.-Q. *Adv. Mater.* **2008**, *20*, 3793–3810. (b) Ma, W.; Iyer, P. K.; Gong, X.; Liu, B.; Moses, D.; Bazan, G. C.; Heeger, A. J. *Adv. Mater.* **2005**, *17*, 274–277.

(3) (a) McQuade, D. T.; Pullen, A. E.; Swager, T. M. *Chem. Rev.* **2000**, *100*, 2537–2574. (b) Thomas, S. W., III; Joly, G. D.; Swager, T. M. *Chem. Rev.* **2007**, *107*, 1339–1386.

(4) (a) Liu, B.; Bazan, G. C. *Proc. Natl. Acad. Sci.* **2005**, *102*, 589–593. (b) Surin, M.; Janssen, P. G. A.; Lazzaroni, R.; Leclere, P.; Meijer, E. W.; Schenning, A. P. H. J. *Adv. Mater.* **2009**, *21*, 1126–1130. (c) Wosnick, J. H.; Mello, C. M.; Swager, T. M. *J. Am. Chem. Soc.* **2005**, *127*, 3400–3405. (d) Tapia, M. J.; Monserín, M.; Valente, A. J. M.; Burrows, H. D.; Mallavia, R. *Adv. Colloid Interface Sci.* **2010**, *158*, 94–107.

(5) (a) Kawase, T.; Shimoda, T.; Newsome, C.; Sirringhaus, H.; Friend, R. H. *Thin Solid Films* **2003**, *438*−*439*, 279–287. (b) Tekin, E.; Smith, P. J.; Schubert, U. S. *Soft Matter* **2008**, *4*, 703–713.

(6) Lukkari, J.; Salomäki, M.; Viinikanoja, A.; Ääritalo, T.; Paukkunen, J.; Kocharova, N.; Kankare, J. *J. Am. Chem. Soc.* **2001**, *123*, 6083–6091.

(7) Zhai, L.; McCullough, R. D. *Adv. Mater.* **2002**, *14*, 901–905.

(8) (a) Bolognesi, A.; Bajo, G.; Geng, Z.; Porzio, W.; Speroni, F. *Thin Solid Films* **1994**, *243*, 683–686. (b) Breiby, D. W.; Samuelsen, E. J.; Konovalov, O.; Struth, B. *Langmuir* **2004**, *20*, 4116–4123. (c) Reitzel, N.; Greve, D. R.; Kjaer, K.; Howes, P. B.; Jayaraman, M.; Savoy, S.; McCullough, R. D.; McDevitt, J. T.; Bjørnholm, T. *J. Am. Chem. Soc.* **2000**, *122*, 5788–5800. (d) Stockton, W. B.; Rubner, M. F. *Macromolecules* **1997**, *30*, 2717–2725.

(9) Joly, G. D.; Geiger, L.; Kooi, S. E.; Swager, T. M. *Macromolecules* **2006**, *39*, 7175–7177.

(10) (a) Burrows, H. D.; Tapia, M. J.; Fonseca, S. M.; Valente, A. J. M.; Lobo, V. M. M.; Justino, L. L. G.; Qiu, S.; Pradhan, S.; Scherf, U.; Chattopadhyay, N.; Knaapila, M.; Garamus, V. M. *ACS Appl. Mater. Interfaces* **2009**, *1*, 864–874. (b) Wågberg, T.; Liu, B.; Orädd, G.; Eliasson, B.; Edman, L. *Eur. Polym. J.* **2009**, *45*, 3230–3235. (c) Wang, H.; Lu, P.; Wang, B.; Qiu, S.; Liu, M.; Hanif, M.; Cheng, G.; Liu, S.; Ma, Y. *Macromol. Rapid Commun.* **2007**, *28*, 1645–1650.

(11) Jiang, H.; Taranekar, P.; Reynolds, J. R.; Schanze, K. S. *Angew. Chem., Int. Ed.* **2009**, *48*, 4300–4316.

(12) Beckers, E. H. A.; Jonkheijm, P.; Schenning, A. P. H. J.; Meskers, S. C. J.; Janssen, R. A. J. *ChemPhysChem* **2005**, *6*, 2029–2031.

(13) Crispin, X.; Jakobsson, F. L. E.; Crispin, A.; Grim, P. C. M.; Andersson, P.; Volodin, A.; van Haesendonck, C.; Van der Auweraer, M.; Salaneck, W. R.; Berggren, M. *Chem. Mater.* **2006**, *18*, 4354–4360.

(14) (a) Burrows, H. D.; Lobo, V. M. M.; Pina, J.; Ramos, M. L.; Seixas de Melo, J.; Valente, A. J. M.; Tapia, M. J.; Pradhan, S.; Scherf, U. *Macromolecules* **2004**, *37*, 7425–7427. (b) Chen, L.; Xu, S.; McBranch, D.; Whitten, D. *J. Am. Chem. Soc.* **2000**, *122*, 9302–9303. (c) Knaapila, M.; Almásy, L.; Garamus, V. M.; Pearson, C.; Pradhan, S.; Petty, M. C.; Scherf, U.; Burrows, H. D.; Monkman, A. P. *J. Phys. Chem. B* **2006**, *110*, 10248–10257. (d) Lavigne, J. J.; Broughton, D. L.; Wilson, J. N.; Erdogan, B.; Bunz, U. H. F. *Macromolecules* **2003**, *36*, 7409–7412.

water. The solubility and subsequent optical effects such as fluorescence enhancement[14a] and change in color, so-called surfactochromism as introduced by Lavigne and Bunz et al.,[14d] can be controlled without synthesizing a series of polymers but simply by varying the surfactant fraction. This has further implications for biosensing, where the surfactant enhances the polymer's role as an emissive donor and may improve both sensitivity and selectivity of the sensor.[16]

Counterion tailoring has a major influence on the water solubility of polythiophenes (PTs) as pioneered by McCullough et al.[17] With increasing counterion size, these authors reported a significant color change from a red aggregated phase to a yellow solution with disrupted aggregates, with the effect resembling the well-known order−disorder transition from an ordered solid of rigid rods to a disordered liquid of more coiled PT chains.[18]

Sodium dodecylsulfate (or sodium lauryl sulfate, SDS) has a well-known micellar structure in water, resolvable by small-angle scattering,[19] with a critical micellar concentration (cmc) ≈ 8.2 mM ≈ 2.4 mg/mL in water.[20] Further structural complexities are obtained for SDS complexes with oppositely charged polyelectolytes[21] or when SDS absorbs onto neutral latex particles.[22] When associated with π-conjugated polymers, SDS has been used to control chemical synthesis of polypyrrole[23] or electrochemical synthesis of PT.[24] Moreover, it forms a dispersion with polyaniline.[25]

Scherf and coworkers have recently introduced a family of π-conjugated block copolymers,[26] including examples of a hydrophobic polyfluorene block such as poly[9,9-bis(2-ethylhexyl)-fluorene] (PF2/6) connected to either a nonionic PT block, for example, poly[3-(6-diethylphosphonatohexyl)thiophene] (P3PHT), or a polyelectrolyte PT block, such as poly[3-(6-trimethylammoniumhexyl)thiophene] (P3TMAHT). The hydrophilic character of the PT blocks leads to solvent-induced self-assembly in mixtures of selective and nonselective solvents including PF2/6-P3PHT in water−tetrahydrofuran or water−hexane[27] or PF2/6-*b*-P3TMAHT in water−tetrahydrofuran[28] or water−methanol.[29] In one example, poly(9,9-dioctylfluorene) (PFO) is coupled to P3TMAHT to form PFO-*b*-P3TMAHT.[30] In water, this polymer shows a small-angle X-ray scattering (SAXS) maximum at $q \approx 0.1$ Å^{-1}, indicating order in solution. The addition of nearly a charge equivalent amount of SDS leads to the disappearance of this maximum and the appearance of a new maximum around $q \approx 0.16$ Å^{-1}. This effect is followed by significant photoluminescence (PL) enhancement of the emission band of PT block, which together point to structural reorganization of P3TMAHT block. The details, however, remain an open question.

In this article, we present a systematic structural study of the homopolymer P3TMAHT with SDS addition in D_2O, thus forming the P3TMAHT(SDS)$_x$ complex (x = the molar ratio of surfactant over monomer units). This article has two objectives. First, whereas the classical picture of McCullough shows the optical transitions of water-soluble PT with the increasing counterion size, we consider the alternative scenario of increasing the counterion fraction where charge balance is also changed. A standard surfactant is employed to make this experiment well controlled and generalized. Second, we use small-angle neutron scattering (SANS) in connection with optical spectroscopy and find phase transitions from ordered P3TMAHT to rod-like (x = 1/5) and sheet-like aggregates (x = 1/2−1), where polymer chains are ordered within the structures, and ellipsoid particles (x = 2−5), which include separated polymer and SDS mantle. Free SDS micelles dominate for higher x. These transitions are followed by distinctive, visibly observable optical changes as transitions from pale red (P3TMAHT) to turbid violet ($x \leq 1$) and orange-yellow ($x \geq 2$). These results reveal for the first time the phase behavior of the P3TMAHT-SDS system, where the optical transitions are induced by changes in the polymer conformation within polymer−surfactant aggregates, whose self-organization is, in turn, controlled simply by varying the surfactant fraction. The results may be readily used to model the behavior of water-soluble PFO-*b*-P3TMAHT-type block copolymers. Generally speaking, whereas there are diverse structural studies of PTs in the solid state (see examples in refs 31 and 32) or organic solvents,[33] less attention has been placed on their water-soluble variants. Our work contributes to the structural understanding of this niche, water-soluble π-conjugated polymers and water-soluble PTs in particular.

Experimental Section

Materials. The synthesis of P3MAHT with a bromide counterion (Chart 1) followed the guidelines described by McCullough.[7] The number-average and weight-average molecular weights were, respectively, M_n = 9.5 kg mol^{-1} and M_w = 12.4 kg mol^{-1}, as measured for polymer precursor with a bromine terminal group (precursor **2** in Scheme 1 in ref 7). Therefore, the degree of polymerization was 40−50. SDS (Chart 1) was purchased from Sigma-Aldrich, and deuterated SDS (SDS-d_{25}) (98.5% D) was purchased from CND Isotopes. These materials were mixed with

(15) (a) Tapia, M. J.; Burrows, H. D.; Valente, A. J. M.; Pradhan, S.; Scherf, U.; Lobo, V. M. M.; Pina, J.; Seixas de Melo, J. *J. Phys. Chem. B.* **2005**, *109*, 19108–19115. (b) Burrows, H. D.; Tapia, M. J.; Silva, C. L.; Pais, A. A. C. C.; Fonseca, S. M.; Pina, J.; Seixas de Melo, J.; Wang, Y.; Marques, E. F.; Knaapila, M.; Monkman, A. P.; Garamus, V. M.; Pradhan, S.; Scherf, U. *J. Phys. Chem. B* **2007**, *111*, 4401–4410.

(16) (a) Al Attar, H. A.; Monkman, A. P. *J. Phys. Chem. B* **2007**, *111*, 12418–12426. (b) Al Attar, H. A.; Norden, J.; O'Brien, S.; Monkman, A. P. *Biosens. Bioelectron.* **2008**, *23*, 1466–1472.

(17) (a) McCullough, R. D.; Ewbank, P. C. *Synth. Met.* **1997**, *84*, 311–312. (b) McCullough, R. D.; Ewbank, P. C.; Loewe, R. S. *J. Am. Chem. Soc.* **1997**, *119*, 633–634.

(18) (a) Tashiro, K.; Ono, K.; Minagawa, Y.; Kobayashi, M.; Kawai, T.; Yoshino, K. *J. Polym. Sci., Part B: Polym. Phys.* **1991**, *29*, 1223–1233. (b) Winokur, M. J.; Spiegel, D.; Kim, Y.; Hotta, S.; Heeger, A. J. *Synth. Met.* **1989**, *28*, C419–C426.

(19) Zemb, T.; Charpin, P. *J. Phys.* (*Paris*) **1985**, *46*, 249–256.

(20) Mukerjee, P.; Mysels, K. J. *Critical Micelle Concentration of Aqueous Surfactant Systems*; National Bureau of Standards: Washington, DC, 1970.

(21) (a) Bastardo, L. A.; Garamus, V. M.; Bergsröm, M.; Claesson, P. M. *J. Phys. Chem. B* **2005**, *109*, 167–174. (b) Bergström, L. M.; Kjellin, U. R. M.; Claesson, P. M.; Grillo, I. *J. Phys. Chem. B* **2004**, *108*, 1874–1881.

(22) Bolze, J.; Hörner, K. D.; Ballauff, M. *Colloid Polym. Sci.* **1996**, *274*, 1099–1108.

(23) Zhang, X. T.; Zhang, J.; Song, W. H.; Liu, Z. F. *J. Phys. Chem. B* **2006**, *110*, 1158–1165.

(24) (a) Bazzaoui, E. A.; Aeiyach, S.; Lacaze, P. C. *Synth. Met.* **1996**, *83*, 159–165. (b) Sakmeche, N.; Aeiyach, S.; Aaron, J.-J.; Jouini, M.; Lacroix, J. C.; Lacaze, P.-C. *Langmuir* **1999**, *15*, 2566–2574.

(25) Gangopadhyay, R. *J. Colloid Interface Sci.* **2009**, *338*, 435–443.

(26) (a) Scherf, U.; Adamczyk, S.; Gutacker, A.; Koenen, N. *Macromol. Rapid Commun.* **2009**, *30*, 1059–1065. (b) Scherf, U.; Gutacker, A.; Koenen, N. *Acc. Chem. Res.* **2008**, *41*, 1086–1097.

(27) Tu, G.; Li, H.; Forster, M.; Heiderhoff, R.; Balk, L. J.; Sigel, R.; Scherf, U. *Small* **2007**, *3*, 1001–1006.

(28) Knaapila, M.; Evans, R. C.; Gutacker, A.; Garamus, V. M.; Torkkeli, M.; Adamczyk, S.; Forster, M.; Scherf, U.; Burrows, H. D. *Langmuir* **2010**, *26*, 5056–5066.

(29) Gutacker, A.; Koenen, N.; Scherf, U.; Adamczyk, S.; Pina, J.; Fonseca, S. M.; Valente, A. J. M.; Evans, R. C.; de Melo, J. S.; Burrows, H. D.; Knaapila, M. *Polymer* **2010**, *51*, 1898–1903.

(30) Gutacker, A.; Adamczyk, S.; Helfer, A.; Garner, L. E.; Evans, R. C.; Fonseca, S. M.; Knaapila, M.; Bazan, G. C.; Burrows, H. D.; Scherf, U. *J. Mater. Chem.* **2010**, *20*, 1423–1430.

(31) (a) Chabinyc, M. L.; Toney, M. F.; Kline, R. J.; McCulloch, I.; Heeney, M. *J. Am. Chem. Soc.* **2007**, *129*, 3226–3237. (b) DeLongchamp, D. M.; Kline, R. J.; Jung, Y.; Lin, E. K.; Fischer, D. A.; Gundlach, D. J.; Cotts, S. K.; Moad, A. J.; Richter, L. J.; Toney, M. F.; Heeney, M.; McCulloch, I. *Macromolecules* **2008**, *41*, 5709–5715. (c) Sirringhaus, H.; Brown, P. J.; Friend, R. H.; Nielsen, M. M.; Bechgaard, K.; Langeveld-Voss, B. M. W.; Spiering, A. J. H.; Janssen, R. A. J.; Meijer, E. W.; Herwig, P.; de Leeuw, D. M. *Nature* **1999**, *401*, 685–688.

(32) Prosa, T. J.; Winokur, M. J.; Moulton, J.; Smith, P.; Heeger, A. J. *Macromolecules* **1992**, *25*, 4364–4372.

(33) Yamamoto, T.; Komarudin, D.; Arai, M.; Lee, B.-L.; Suganuma, H.; Asakawa, N.; Inoue, Y.; Kubota, K.; Sasaki, S.; Fukuda, T.; Matsuda, H. *J. Am. Chem. Soc.* **1998**, *120*, 2047–2058.

Chart 1. Chemical Structures of P3TMAHT Polymer (n = 40−50) and SDS Surfactant

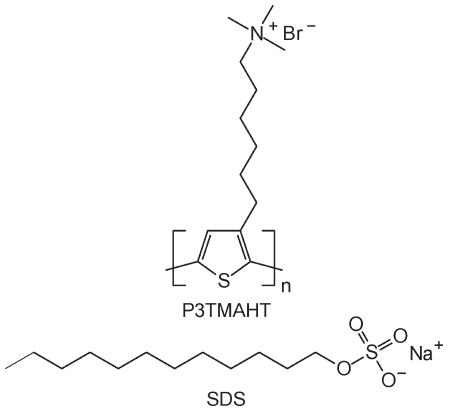

D_2O (99.9% D, Cambridge Isotope Laboratories, Inc.). We prepared P3TMAHT(SDS)$_x$−D_2O mixtures, where x stands for the molar ratio of SDS over P3TMAHT monomers, by mixing 10 mg/mL P3TMAHT−D_2O solution, where the concentration is given with respect to the P3TMAHT monomer units, with 10.55 mg/mL SDS−D_2O solution so that the desired molar ratio x was reached. The value x = 1 corresponds to the stoichiometric charge balance. The compositions of polymer−surfactant complexes studied by small-angle scattering and initial optical measurements are given in Table 1.

Instrumentation and Methods. Photographs of the samples were taken using a Canon Ixus digital camera.

SANS measurements of P3TMAHT, SDS, and P3TMAHT-(SDS)$_x$ in D_2O were performed on the *Yellow Submarine* instrument at the BNC in Budapest (Hungary).[34] SANS measurements of P3TMAHT(SDS-d_{25})$_x$ in D_2O were performed at the SANS-1 instrument at the GKSS Research Centre in Geesthacht (Germany).[35] The overall q range was from 0.004 to 0.4 Å^{-1}. In both cases, the samples were filled in Hellma quartz cells of 2 mm path length and placed in a thermostated holder. The raw scattering patterns were corrected for sample transmission, background, and sample cell scattering. The isotropic 2-D scattering patterns were azimuthally averaged, converted to an absolute scale, and corrected for detector efficiency by dividing by the incoherent scattering spectra of 1 mm thick pure water. The scattering from a mixture of D_2O and water (99:1) was subtracted as the background. The small incoherent scattering due to nondeuterated polymer was taken into account by the fitting procedure. All measurements were performed at 20.0 ± 0.5 °C.

SAXS experiments of P3TMAHT and P3TMAHT(SDS)$_x$ in D_2O were performed at the I711 beamline at MAX-lab in Lund (Sweden).[36] The X-ray energy was 11.3 keV, and the sample-to-detector distance was 1.3 m, yielding a q range of 0.01 to 0.2 Å^{-1}. The beam size was 0.30 × 0.30 mm^2 (vert. × hor.). The scattering patterns were measured using a MarCCD165 detector. The intensity scale was calibrated using water.

UV/vis absorption and photoluminescence (PL) measurements of P3TMAHT(SDS)$_x$−D2O were performed using a Perkin-Elmer Lambda 1050 UV/vis/NIR spectrophotometer and a HORIBA Jobin Yvon Fluorolog-3 fluorimeter, respectively. The measurements were first performed on the same samples used for scattering measurements to enable direct comparison. Additional measurements were made on samples diluted by a factor of 100 in water (i.e., total concentration ∼0.1 mg/mL (or ∼0.01 vol %)). In dilute samples, the SDS concentration is below the cmc of pure SDS in water, but the molar ratio x for a given sample is unaltered.

Table 1. Composition of P3TMAHT(SDS)$_x$−D_2O and P3TMAHT(SDS-d_{25})$_x$−D_2O Samples

x	monomer concn. (mg/mL)	SDS concn (mg/mL)	SDS-d_{25} concn (mg/mL)	overall concn (mg/mL)
1/5	8.33	1.76		10.09
1/5	8.33		1.62	9.95
1/2	6.67	3.52		10.18
1/2	6.67		3.24	9.90
1	5.00	5.28		10.28
1	5.00		4.85	9.85
2	3.33	7.03		10.37
5	1.67	8.79		10.46
5	1.67		8.09	9.75
20	0.48	10.05		10.53

The elevated concentrations used in scattering measurements exceeded the recommended concentration regime for optical spectroscopy (∼10^{-5}−10^{-8} M). We therefore anticipated considerable difficulties in our measurements due to both saturation of the detector and self-absorption. To eliminate these problems to some extent, samples were measured in short-path-length (1 mm) quartz cuvettes. For UV/vis absorbance the reference beam was attenuated using an in-built neutral density filter (1% T). For PL measurements, the signal intensity was attenuated manually using a neutral density filter (λ > 400 nm O.D. ≈ 0.35, λ < 364 nm O.D. ≈ 0.55).

Analysis of Scattering Data. The scattering functions were interpreted using scaling concepts. This simple interpretation was enhanced by numerical modeling to certain geometric shapes using the indirect Fourier transformation (IFT) programs GNOM[37] and Glatter[38] This allowed the evaluation of particle shape in terms of simulated annealing with DAMMIF.[39]

Selected data sets of the supposedly highly asymmetric particles show a deviation between the experimental data and the curves calculated from the IFT analysis. This deviation was interpreted as a crossover from rigid to flexible particles. In this analysis, we considered scattering intensity as

$$\frac{1}{c}\frac{\mathrm{d}\sum(q)}{\mathrm{d}\Omega} \approx q^{-\alpha} \qquad (1)$$

where c is concentration and α is the scattering power of the considered particles. Cylindrical particles would lead to the scattering power α = 1 for $l_p^{-1} < q < R_{cs}^{-1}$, where l_p and R_{CS} are the persistence length and the cross section of particles. The coiled particles are assumed to show α = 2 for $L^{-1} < q < l_p^{-1}$, where L is the contour length of the particles.

When the data indicated a crossover from α = 1 to 2, the data were further analyzed using both a Gaussian chain model as well as direct modeling of Pedersen.[40] In the latter modeling, the flexibility of the long aggregates or polymers is estimated by considering simultaneously both parts of the scattering curve (below and above the crossover point). The scattering intensity of such semiflexible particles is[40]

$$\frac{1}{c}\frac{\mathrm{d}\sum(q)}{\mathrm{d}\Omega} \approx S_{WC}(q, L, l_p)S_{CS}(q, a, b) \qquad (2)$$

where $S_{WC}(q,L,l_p)$ is the single chain scattering function for a semiflexible chain including excluded-volume effects of l_p and L.

(34) Rosta, L. *Appl. Phys. A: Mater. Sci. Process.* **2002**, *74*, S52–S54.
(35) Stuhrmann, H. B.; Burkhardt, N.; Dietrich, G.; Jünemann, R.; Meerwinck, W.; Schmitt, M.; Wadzack, J.; Willumeit, R.; Zhao, J.; Nierhaus, K. H. *Nucl. Instrum. Methods Phys. Res., Sect. A* **1995**, *356*, 124–132.
(36) Knaapila, M.; Svensson, C.; Barauskas, J.; Zackrisson, M.; Nielsen, S. S.; Toft, K. N.; Vestergaard, B.; Arleth, L.; Olsson, U.; Pedersen, J. S.; Cerenius, Y. *J. Synchrotron Radiat.* **2009**, *16*, 498–504.
(37) Svergun, D. I. *J. Appl. Crystallogr.* **1992**, *25*, 495–503.
(38) Glatter, O. *J. Appl. Crystallogr.* **1977**, *10*, 415–421.
(39) Franke, D.; Svergun, D. I. *J. Appl. Crystallogr.* **2009**, *42*, 342–346.
(40) (a) Jerke, G.; Pedersen, J. S.; Egelhaaf, S. U.; Schurtenberger, P. *Phys. Rev. E* **1997**, *56*, 5772–5788. (b) Pedersen, J. S.; Schurtenberger, P. *Macromolecules* **1996**, *29*, 7602–7612.

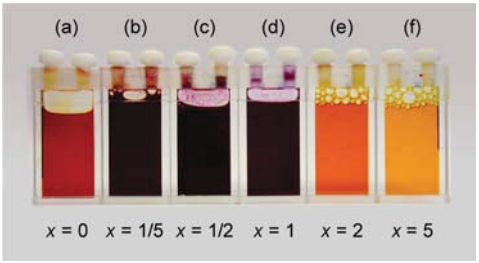

Figure 1. Photograph of P3TMAHT(SDS)$_x$−D_2O for x = (a) 0, (b) 1/5, (c) 1/2, (d) 1, (e) 2, and (f) 5 at room temperature.

S_{CS} (q,a,b) represents the scattering of the elliptical cross section of the semiflexible aggregates.

Results and Discussion

Visual Considerations. Figure 1 shows a photograph of P3TMAHT(SDS)$_x$ in D_2O as a function of molar ratio, x. Pure P3TMAHT powder is red, and the color is maintained when the polymer is dissolved in D_2O. The solution turns purple on SDS addition at concentrations below the nominal charge compensation point (i.e., when $x \leq 1$). When the SDS concentration exceeds this point ($x > 1$), the solution gradually becomes yellow. P3TMAHT forms a transparent solution with D_2O and with high concentrations of SDS ($x \geq 2$), but some precipitation occurs for x = 1/2 to 1.

The color change from purple to yellow is similar to that reported by McCullough for HT-2,5-poly(thiophene-3-propionic acid) when the counterion size is changed from small to large.[17] These authors also found a similar tendency with increasing counterion fraction (for NH_4OH). The observed precipitation for P3TMAHT(SDS)$_{1.0}$ is also analogous to the lysozyme−SDS system.[41] Both lysozyme and oppositely charged SDS are independently water-soluble but form a self-organized complex together. At the charge neutralization point, these complexes form a system of dissolved and precipitated phases in equilibrium with each other.

The solvatochromicity reported by McCullough[17] was understood in terms of self-assembly (purple) and disassembly (yellow). It seems plausible that the changes observed for P3TMAHT(SDS)$_x$−D_2O must also stem from significant structural alterations. To study these alterations we carried out solution scattering experiments.

Solution Structure. *Pure Compounds in D_2O: SANS Experiments*. Pure compounds were used as a prelude for polymer−surfactant complex experiments. Figure 2a plots SANS patterns of P3TMAHT−D_2O at various concentrations. The data are dominated by an upturn at low q (< 0.01 Å^{-1}) and a broad interference maximum at higher q (~0.04 Å^{-1}). The length of the thiophene monomer is ~4 Å,[32] and thus the length of a single P3TMAHT polymer chain is 160−200 Å. This value falls below the upper limit of our observation window (~800 Å); therefore, if the polymer was dissolved down to the molecular level, then the SANS curve would level off as a Guinier plateau at experimentally attainable q. Since no such plateau is observed but instead there is an upturn, this indicates the presence of polymer associations. Figure 2b plots the position of the interference maximum as a function of concentration. As the peak moves toward higher q with increasing concentration, this points to order between the polymer associations. The peak position scales as

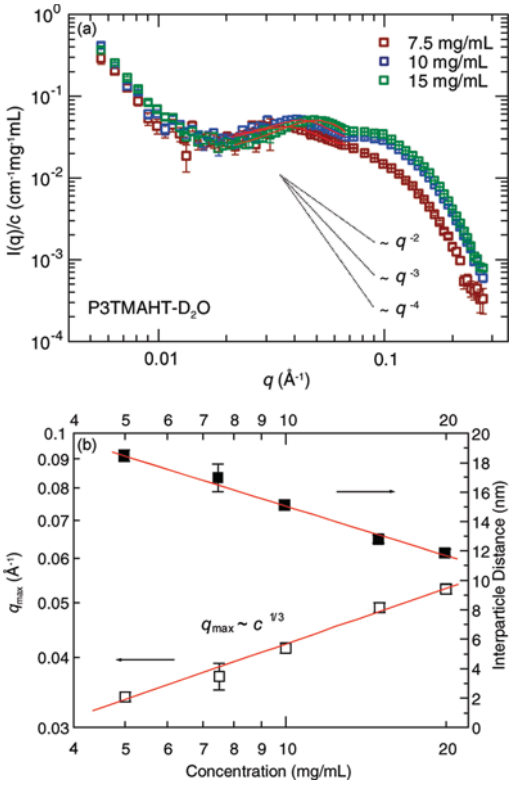

Figure 2. (a) SANS data of P3TMAHT−D_2O at concentrations 7.5 mg/mL (open brown squares), 10 mg/mL (open blue squares), and 15 mg/mL (open green squares). The curves are normalized to concentration. Red lines are fits to the interference maxima, as described in the text. Dashed lines show −2, −3, and −4 decays for comparison. (b) Position of the observed interference maximum (q_{max}) and the corresponding distance between P3TMAHT aggregates as a function of concentration. The data points at 5 and 20 mg/mL are taken from ref 28. T = 20 °C.

$q_{max} \approx c^{0.32\pm0.02} \approx c^{1/3}$, which is indicative of aggregates ordered in a 3-D array.[42]

The SANS patterns of the SDS−D_2O systems used in this study are shown in the Supporting Information. The lower concentration equals the nominal SDS concentration (5.28 mg/mL) in the studied polymer complexes at the nominal charge compensation point (vide infra). The higher concentration corresponds to the equivalent overall concentration of polymer−SDS complexes (~10 mg/mL). Both samples exceed the surfactant cmc in water (~2.4 mg/mL).[20] The data are consistent with the well-described SANS data of SDS−D_2O[19] with a broad maximum at 0.04 to 0.05 Å^{-1}; the feature stems from intermicellar interactions, its position scaling with concentration.

P3TMAHT(SDS)$_x$ and P3TMAHT(SDS-d_{25})$_x$ in D_2O: SANS Experiments. Figure 3 plots SANS patterns of P3TMAHT(SDS)$_x$−D_2O for $x \leq 1$, that is, when the molar ratio is less than or equal to the nominal charge compensation point (Figure 3a), and for $x > 1$, that is, when the ratio exceeds this point (Figure 3b). The data of P3TMAHT−D_2O and SDS−D_2O are shown for comparison, along with selected model fits using both softwares GNOM and Glatter (black and orange lines, respectively). The SDS concentration exceeds its cmc in water in all cases except for the sample x = 1/5. The SANS data of

(41) Morén, A. K.; Khan, A. *Langmuir* **1995**, *11*, 3636–3643.

(42) (a) Boden, N. Micellar Liquid Crystals. In *Micelles, Membranes, Microemulsions, And Monolayers*; Gelbart, W. M., Ben-Shaul, A., Roux, D., Eds.; Springer: New York, 1994; pp 153−211. (b) Chen, S. H.; Sheu, E. Y.; Kalus, J.; Hoffman, H. *J. Appl. Crystallogr.* **1988**, *21*, 751–769.

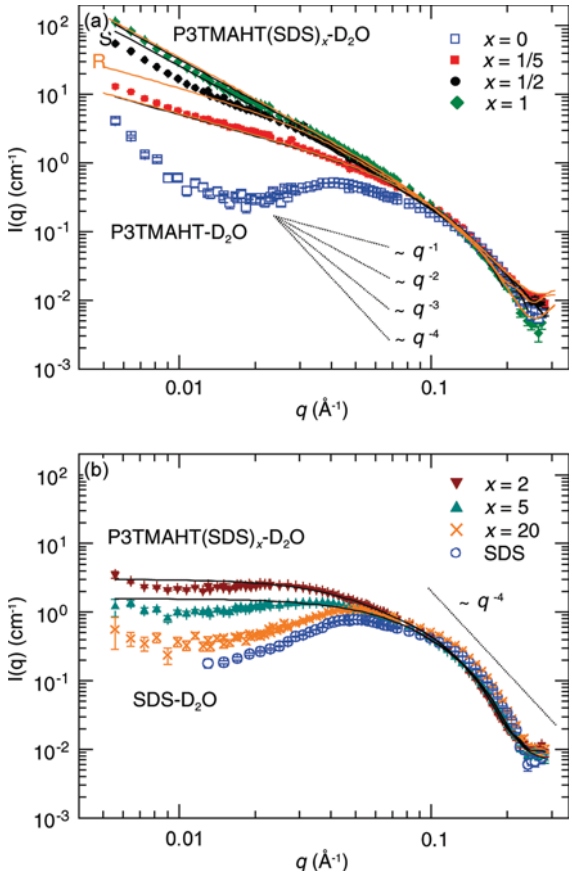

Figure 3. (a) SANS data of P3TMAHT−D_2O (open blue squares) and P3TMAHT(SDS)$_x$−D_2O below the nominal charge compensation point: $x = 1/5$ (solid red squares), $x = 1/2$ (solid black spheres), and $x = 1$ (solid green diamonds). (b) SANS data of SDS−D_2O (open blue circles) and P3TMAHT(SDS)$_x$−D_2O above the nominal charge compensation point: $x = 2$ (solid brown down triangles), $x = 5$ (solid cyan up triangles), and $x = 20$ (orange crosses). The black and orange solid lines represent structural models fitted to the data. "S" and "R" (a) denote fits to the alternative sheet-like and rod-like models for $x = 1/2$. (See the text for details). Dotted lines show the ideal slopes for comparison. The overall concentration was ~10 mg/mL for each case. $T = 20$ °C.

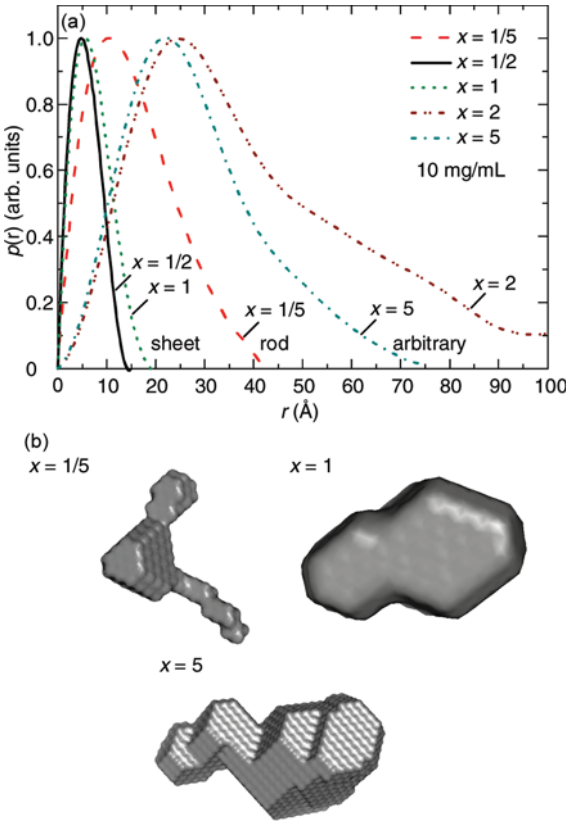

Figure 4. (a) Examples of distance distribution functions as estimated from the SANS data of P3TMAHT(SDS)$_x$−D_2O for $x = 1/5$ (dashed red line) using an elongated rod-like particle model; for $x = 1/2$ (solid black line) and $x = 1$ (dotted green line) using a sheet-like particle model; and for $x = 2$ (brown dashed and double-dotted line) and $x = 5$ (cyan dashed−dotted line) using a model where the particle shape can be arbitrary. These functions correspond to the fits shown in Figure 3. The overall concentration of all samples was ~10 mg/mL. (b) "Top-view" examples obtained from the corresponding data by simulated annealing.

P3TMAHT are significantly altered by SDS addition and do not resemble either those of the pure constituents or their superposition, which indicates the formation of completely new self-organized structures. The scattering power estimated from these data gives us a putative idea of the particle shape. Further information on the shape was extracted from the weighted autocorrelation function of the particle contrast of neutron scattering lengths density in heavy water, known as the distance distribution function $p(r)$. The obtained functions as well as the simulated particle shapes obtained for selected systems are shown in Figure 4. Essential structural parameters estimated from these data are compiled in Table 2.

Figure 3a shows that the scattering intensities of P3TMAHT-(SDS)$_x$−D_2O increase up to $x = 1$. This is likely to be the point of charge compensation between the polymer and surfactant. Charge balance diminishes the water solubility and leads to partial phase separation, visually observed as precipitation, the extent of which, however, is less than the total amount of material (Figure 1a). All data show a nearly monotonous decay for ~0.004 to 0.06 Å^{-1}. This decay varies with increasing x from −1 ($x = 1/5$) to −2 ($x = 1$) and is associated with the 10-fold increase in scattering intensity. At higher q, the data show a shallow downturn (for > 0.06 Å^{-1}) approaching a −4 decay (> 0.1 Å^{-1}) for all x, the intensity level staying nearly constant. Unlike the case of P3TMAHT−D_2O, no interference maxima are observed for P3TMAHT(SDS)$_x$−D_2O. These data give us an idea of the formation of stiff rod-like ($x = 1/5$), sheet-like ($x = 1$), and possibly worm-like ($x = 1/2$) polymer−surfactant associations without interparticle order. The lateral size of these aggregates reaches up to the 800 Å window or beyond. The diameter of rod-like aggregates corresponds to polymer surfactant bilayers (~40 Å). In contrast, the sheets appear very thin (~20 Å) corresponding to the solid-state d-spacing of poly(3-octylthiophene),[32] thus basically to a single polymer layer. Both sheet-like and rod-like models may be fitted to the data for $x = 1/2$, but both models deviate at the lowest q values. These models are marked by "S" and "R" in Figure 3a. The asymmetrical shape of the $p(r)$ function calculated from the rod-like model implies a transition from rods to sheets (Figure 4a and Supporting Information).

Figure 3b shows that the scattering intensities of P3TMAHT-(SDS)$_x$−D_2O are significantly reduced for $x > 1$. No signs of large rod-like or sheet-like aggregates are seen, but the data are reminiscent of 3-D aggregates with finite lateral size (~100 Å). Since the data are not far from those of pure SDS, this situation could point to macrophase separation of polymer after the charge neutralization point, with the scattering arising purely from SDS

Table 2. Essential Structural Parameters Obtained from the SANS Data for P3TMAHT(SDS)$_x$−D$_2$O and P3TMAHT(SDS-d_{25})$_x$−D$_2$O by Indirect Methods[a]

x	analyzed q-range	α	model	D_{max} (Å)	$R_{CS,g}$ (Å)	$R_{T,g}$ (Å)	R_g (Å)
			With SDS				
1/5	0.006 to 0.06	1.25 ± 0.03					
	0.006 to 0.28		rod	42	12.5 ± 0.1		
	0.006 to 0.28		rod*	42	13.3 ± 0.2		
	0.006 to 0.28		rod*	79	18.5 ± 0.1		
1/2	0.006 to 0.06	1.69 ± 0.02					
	0.006 to 0.28		sheet	15		4.6 ± 0.1	
	0.006 to 0.28		rod*	99	28 ± 1		
1	0.006 to 0.06	1.94 ± 0.01					
	0.006 to 0.28		sheet	19		5.7 ± 0.1	
	0.006 to 0.28		sheet*	20		6.6 ± 0.1	
2	0.006 to 0.28	n/a	arbit.	100			32.2 ± 0.2
5	0.006 to 0.28	n/a	arbit.	75			22.3 ± 0.1
			With SDS-d_{25}				
1/5	0.006 to 0.018	2.05 ± 0.06					
	0.018 to 0.08	1.10 ± 0.03					
	0.018 to 0.20		rod	40	11.6 ± 0.1		
	0.006 to 0.24		rod*	39	11.9 ± 0.2		
1/2	0.006 to 0.018	2.22 ± 0.03					
	0.018 to 0.08	1.14 ± 0.02					
	0.006 to 0.24		rod*	44	14.2 ± 0.1		
	0.006 to 0.24		rod*	99	22.0 ± 0.5		
1	0.006 to 0.018	2.95 ± 0.02					
	0.018 to 0.08	1.97 ± 0.03					
	0.006 to 0.20		sheet	20		6.2 ± 0.1	
	0.006 to 0.24		sheet*	20		7.3 ± 0.1	
5	0.018 to 0.08	1.07 ± 0.04					
5	0.011 to 0.25	1.25 ± 0.03	rod*	44	15.6 ± 0.4		

[a] α, D_{max}, $R_{CS,g}$, $R_{T,g}$, and R_g, are, respectively, the scattering power, considered maximum size of the particle (rod diameter, sheet thickness, or particle size), the radius of gyration for the cross section of a cylindrical particle, for the thickness of a sheet-like particle or for the whole arbitrary-shaped particle. The values are estimated using GNOM [ ] or Glatter [*].

micelles. However, no interference maximum is seen for $x = 2$, and only remnants are observable for $x = 5$. This means that some polymer must be incorporated into or alternatively absorbed onto the surfactant associations and screen electrostatic interactions. The second explanation is a significant release of free ions due to the formation of P3TMAHT(SDS)$_x$ complexes, which leads to good screening of electrostatic interaction between micelles. For $x = 20$, the data approach that of pure SDS with an interference maximum that indicates the dominance of pure or nearly pure SDS micelles.

To study the internal structure of these aggregates further, we performed SANS experiments with deuterated SDS. Figure 5 plots SANS patterns of P3TMAHT(SDS-d_{25})$_x$−D$_2$O for x = 1/5 to 5 normalized to the monomer concentrations. Because the contrast difference is significantly higher between P3TMAHT and D$_2$O than between SDS-d_{25} and D$_2$O, the scattering mainly arises from the polymer contribution within the expected polymer−surfactant associations. Also shown are fits to the models obtained using softwares GNOM and Glatter (black and orange lines). The data of the pure polymer are shown for comparison. Structural parameters calculated from these data are collected in Table 2. As expected, the scattering intensities of all samples are reduced, this effect increasing with x, which is in agreement with the idea of P3TMAHT−SDS aggregates.

When considering the case $x = 1/5$, the data show a −2 decay below ∼0.018 Å^{-1} (≡ q^*) and a −1 decay above it. This turning point is best shown in a Holtzer plot (Supporting Information). At first sight, this is indicative of rod-like polymers turning into Gaussian coils at longer distances. The corresponding persistence length (l_p) would be ∼190 Å, if determined from the relation $q^* l_p \approx 3.5$.[43] The case $x = 1/2$ resembles $x = 1/5$, but the slopes

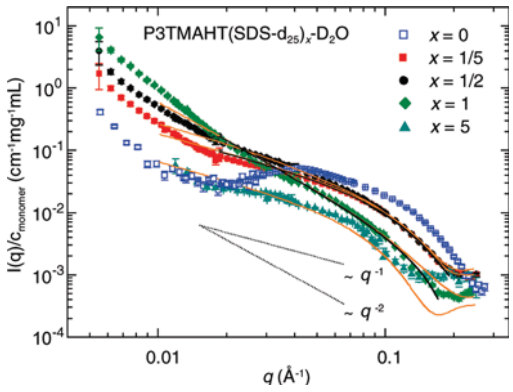

Figure 5. SANS data of P3TMAHT-D$_2$O (open blue squares) and P3TMAHT(SDS-d_{25})$_x$−D$_2$O for x = 1/5 (solid red squares), x = 1/2 (solid black spheres), x = 1 (solid green diamonds), and x = 5 (solid cyan up triangles). The black and orange solid lines represent models fitted to the data. (See the text for details.) Dotted black lines show −1 and −2 decays for comparison. The overall concentration was ∼10 mg/mL. T = 20 °C.

deviate further from the ideal −2 and −1 behavior. As the obtained persistence length exceeds the length of a single P3TMAHT chain, these data indicate the situation where rod-like (x = 1/5) or sheet-like (x = 1/2) P3TMAHT(SDS-d_{25})$_x$ aggregates contain P3TMAHT

(43) Lecommandoux, S.; Chécot, F.; Borsali, R.; Schappacher, M.; Deffieux, A.; Brûlet, A.; Cotton, J. P. *Macromolecules* **2002**, *35*, 8878–8881.This is a semiempirical definition and valid for bottle-brush polymers with the length ≫ l_p (Hsu, H.-P.; Paul, W.: Binder, K. *Macromolecules* **2010**, *43*, 3094−3102). However, we may actually consider polymer associations.

associations (and not separated polymer chains) that can bend within the polymer−surfactant aggregates.

The case $x = 1$ shows a scattering curve following approximately a −2 decay for the whole q-range. This indicates the existence of sheet-like polymer associations within sheet-like polymer−surfactant aggregates. For $x = 5$, the scattering curve follows a −1 decay, thus indicating the presence of dissolved rod-like polymers either incorporated into or absorbed onto ellipsoidal polymer−surfactant aggregates. The scattering level is moreover reduced, which is clearly visible in the height of the Holtzer plateau (Supporting Information). For comb-like brush polymers, this plateau equals πM_L where M_L is the linear mass density.[44] The reduction of M_L is consistent with the idea of separated polymer chains.

The $p(r)$ functions calculated from these data compared with those calculated from the data of P3TMAHT(SDS)$_x$−D_2O (Figure 4) are presented in the Supporting Information. For $x = 1/5$ or 1, the functions show a small shift of the maximum, indicating that the SDS molecules can penetrate inside the polymer template. For $x = 1/2$, the function is very asymmetric. The maxima coexist at ∼15 Å, but there is a large variation at larger r. This indicates narrow polymer domains and significant SDS contribution at larger r, which is consistent with the idea of polymer bundles inside larger polymer−surfactant aggregates.

P3TMAHT(SDS)$_x$ and P3TMAHT(SDS-d_{25})$_x$ in D_2O at Low x Limit: SANS Experiments with a Semiflexible Model. Specific attention is placed on the internal aggregate structure at low x limit. These data show a potential crossover from rod-like to coil-like behavior (eq 1), and this effect is most pronounced inside the aggregates. Figure 6 plots the SANS data of P3TMAHT(SDS)$_x$−D_2O and P3TMAHT(SDS-d_{25})$_x$−D_2O for $x = 1/5$ and 1/2 side by side. The solid lines represent the curves calculated from the models of semiflexible aggregates (eq 2) for the whole q-range with SDS and for the higher q-range (> 0.018 Å^{-1}) with SDS-d_{25}. The low q-range (< 0.018 Å^{-1}) of the data with SDS-d_{25} is fitted to a Gaussian chain model. Structural parameters obtained from these curves are compiled in Table 3. These models give a satisfactory reproduction of the upturn of the scattering data, which points to the flexibility of the aggregates formed. The consideration also indicates that the flexibility of polymer−SDS aggregates is increased (Kuhn length decreased) when increasing x from 1/5 to 1/2. Furthermore, their cross-section becomes more elliptical.

When comparing SANS data of P3TMAHT(SDS-d_{25})$_{1/5}$ and P3TMAHT(SDS)$_{1/5}$, we do not observe major changes at the lowest q (Figure 6a). This scattering thus appears like the trace scattering expected from large aggregates, which is fully consistent with the idea that P3TMAHT is not dissolved but forms bundle-like polymer associations inside the polymer−surfactant aggregates. The second (Gaussian) model component is present in the case of SDS-d_{25} but not in the case of SDS, which implies that part of the surfactant is incorporated into the polymer associations. A similar, though much weaker, tendency is seen for $x = 1/2$ (Figure 6b).

The aggregate stiffness, and thus the persistence length, is influenced by both the interaction within and between the aggregates. Our consideration takes the intra-aggregate interaction into account, but to estimate interaction between aggregates, the data should be extrapolated to the value at "zero concentration". The contour length is influenced by the polydispersity of the aggregates. Although in the present case, the aggregates are likely to be polydisperse, we were not able to determine this prior to

(44) Fischer, K.; Schmidt, M. *Macromol. Rapid Commun.* **2001**, *22*, 787–791.

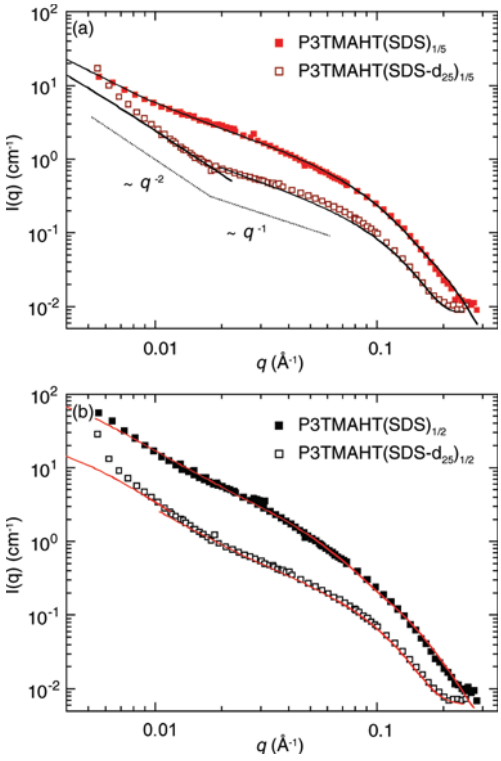

Figure 6. (a) SANS data of P3TMAHT(SDS)$_{1/5}$−D_2O (solid red squares) and P3TMAHT(SDS-d_{25})$_{1/5}$−D_2O (open brown squares). (b) SANS data of P3TMAHT(SDS)$_{1/2}$−D_2O (solid black squares) and P3TMAHT(SDS-d_{25})$_{1/2}$−D_2O (open black squares). Solid lines represent semiflexible models fitted to the data. (See the text for details.) Dotted lines show −2 and −1 decays for comparison.

modeling. Note that the polydispersity of aggregates is not the same as the polydispersity of P3TMAHT.

P3TMAHT and P3TMAHT(SDS)$_x$ in D_2O: SAXS Experiments. Figure 7 plots SAXS patterns of P3TMAHT−D_2O and P3TMAHT(SDS)$_x$−D_2O for $x = 1$ and 5. The data for the pure polymer show an upturn and a broad maximum (∼0.046 Å^{-1}) that compare well to the upturn and maximum (∼0.042 Å^{-1}) seen in the SANS data (Figure 4). The case $x = 1$ is dominated by a monotonous slope of −1.93 to −2, also corresponding to the SANS data. For $x = 5$, the data are, however, different, showing an additional maximum at 0.18 Å^{-1}. Free SDS micelles show an intermicellar SANS peak at 0.04 to 0.05 Å^{-1} and a SAXS peak ∼0.16 Å^{-1} associated with the polar cell of the surfactant head groups.[19] The peak observed for $x = 5$ in SAXS points to the existence of free SDS micelles with a well-defined internal structure, but the absent or significantly weakened SANS peak indicates a lack of intermicellar order, plausibly due to the charge screening of P3TMAHT polymer attached to the micelles.

Photophysical Consequences. Our photophysical studies of P3TMAHT(SDS)$_x$−D_2O have two objectives. First, a significant difference in the visual appearance of the samples (Figure 1) suggests that the surfactant dramatically alters the electronic and optical properties of P3TMAHT, and this "surfactochromism" deserves detailed consideration. Second, the photophysical data provide an indirect probe for the intramolecular structure, thus complementing the above-described scattering experiments and the idea of intermolecular structure. For example, because the relation between optical spectra and π-stacking of PTs in solutions is known,[33] we can obtain an idea of polymer association and separation for each x.

Table 3. Parameters Obtained from the Semi-Flexible and Gaussian Models Fitted to the SANS data for P3TMAHT(SDS)$_x$−D$_2$O and P3TMAHT(SDS-d_{25})$_x$−D$_2$O[a]

x	analyzed q range (Å^{-1})	model	Kuhn length (Å)	R_g (Å)	a (Å)	b (Å)
			With SDS			
1/5	0.006 to 0.3	semiflexible chain	440 ± 40		25 ± 2	10 ± 2
1/2	0.006 to 0.3	semiflexible chain	160 ± 20		40 ± 4	10 ± 2
			With SDS-d_{25}			
1/5	0.006 to 0.018	Gaussian chain		~755		
	0.018 to 0.3	semiflexible chains	380 ± 30		16 ± 2	15 ± 2
1/2	0.006 to 0.018	Gaussian chain		~400		
	0.018 to 0.08	semiflexible chain	150 ± 10		22 ± 2	16 ± 2

[a] For the semiflexible chain, Kuhn length equals $2l_p$. R_g and a and b are, respectively the radius of gyration for the Gaussian chain and the axes of ellipse for the ellipsoidal cross section of the semiflexible chain or particle.

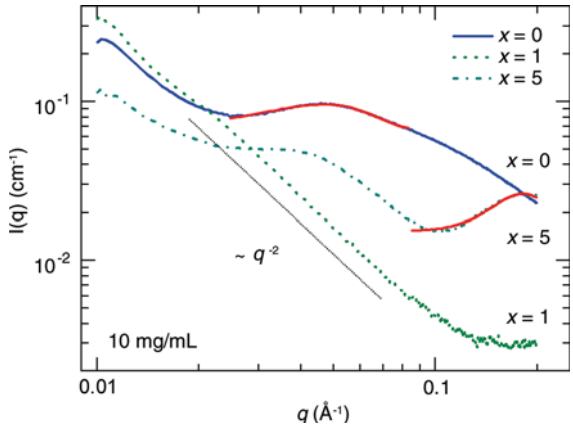

Figure 7. SAXS data of P3TMAHT−D$_2$O (solid blue curve) and P3TMAHT(SDS)$_x$−D$_2$O with x = 1 (dotted green curve) and x = 5 (dashed and dotted cyan curve). Red lines show fits to the apparent interference maxima. The dotted black line shows a −2 decay for comparison. The overall concentration was ~10 mg/mL. $T \approx 20$ °C.

Figure 8 plots the photoabsorption data of P3TMAHT(SDS)$_x$ in D$_2$O as a function of x. Figure 9 plots the corresponding PL data. The absorption and emission maxima are compiled in Table 4. Also shown are the monomer, SDS, and overall concentrations of the studied samples. The data shown in Figures 8a and 9a are obtained from the samples measured using scattering techniques (~10 mg/mL). The data shown in Figures 8b,c and 9b are obtained on dilution of the samples by a factor of 100, which leaves the relative P3TMAHT−SDS mole fraction unchanged but dilutes the SDS concentration below its cmc.

On variation of x, distinct surfactochromatic shifts in the absorption maxima are observed (Figure 8), which become more resolved upon dilution (Figure 8b,c). For x = 0 the UV/vis absorption spectrum is characterized by a broad, featureless band with a maximum at 429 nm. On increasing the SDS mole fraction to 1/5 and then to 1, the maximum is progressively more red-shifted, and the band exhibits vibronic structure. However, between x = 1 and 5, a dramatic hypsochromic (blue) shift in the absorption maximum (to 422 nm) is observed and is accompanied by a loss of the vibronic structure. Moreover, this absorption maximum is blue-shifted further than that observed for P3TMAHT in the absence of SDS, which may indicate that the charge excess of SDS screens P3TMAHT interactions. As shown in Figure 1, the data correspond to a visual color change of the solution from deep red (x = 0) to deep purple (x = 1/5 to 1) to yellow (x = 5). The trends are independent of sample concentration, indicating that they cannot be attributed to the formation of simple SDS micelles. Excitation spectra (Supporting Information) are in agreement with the absorption data for a variety of emission wavelengths (620, 650, and 680 nm).

A qualitative comparison of the absorption efficiency may be achieved by normalizing the spectra relative to the monomer concentration (Figure 8c). The relative integrated absorbance remains constant for all samples with the exception of x = 1, where a dramatic reduction in the absorbance to 20% is observed. The lower absorption of the P3TMAHT(SDS)$_{1.0}$−D$_2$O system may be accounted for by charge compensation, leading to decreased water solubility and eventually visually detectable macrophase separation (Figure 1d) in the formation of a fine precipitate.

The PL spectra of P3TMAHT(SDS)$_x$−D$_2$O on excitation at 430 nm also exhibit clear surfactochromatic effects (Figure 9): a broad featureless band for x = 0, increased band narrowing, and the appearance of vibronic structure on SDS addition from x = 1/5 to 1, followed by the return to a blue-shifted broad emission band for x = 5. In the concentrated samples (Figure 9a), the emission spectra are broader and red-shifted in comparison with the more dilute solutions (Figure 9b), but the surfactochromatic behavior is essentially concentration-independent.

The optical properties of PTs are known to be very responsive to intrachain conformational changes and interchain aggregation.[45] The broad emission band observed for P3TMAHT−D$_2$O is characteristic of PT emission. On addition of SDS (x = 1/5 to 1), the emission spectrum changes dramatically, resolving into a narrower emission band with clear vibronic structure ($\Delta E \approx 0.15$ eV), which is assigned to the vibronic progression of the C=C stretching mode.[46] The Stokes shifts are calculated to be 0.32 and 0.08 eV for x = 1/5 and 1, respectively. The vibronic structure along with the small Stokes shift suggests that the polymer adopts a more planar, ordered conformation in the presence of SDS, which prevents free rotation of the polymer backbone. This effect is most pronounced for x = 1, consistent with the idea of forming the most planar system, 2-D lamellar sheets or disks, in this concentration regime. Therefore, the data support the idea of formation of structured P3TMAHT(SDS)$_x$ complexes for x = 1/5 and 1.

On addition of further SDS (x = 5), the emission band loses its vibronic structure and reverts back to the broad emission band seen for P3TMAHT−D$_2$O, suggesting the return to a more

(45) Stokes, K. K.; Heuzé, K.; McCullough, R. D. *Macromolecules* **2003**, *36*, 7114–7118.
(46) Sundberg, M.; Inganäs, O.; Stafström, S.; Gustafsson, G.; Sjögren, B. *Solid State Commun.* **1989**, *71*, 435–439.

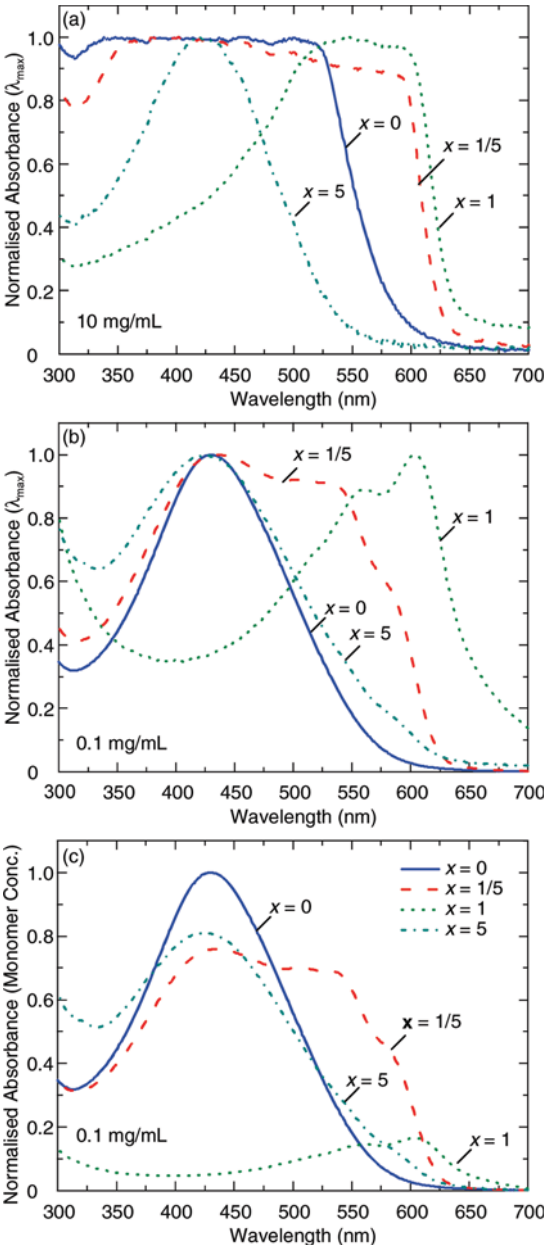

Figure 8. Photoabsorption data of P3TMAHT−D_2O (solid blue curve) and P3TMAHT(SDS)$_x$−D_2O for x = 1/5 (dashed red curve), x = 1 (dotted green curve), and x = 5 (dashed and dotted cyan curve) at ~20 °C. The overall concentration was (a) ~10 or (b,c) ~0.1 mg/mL. The data are normalized to the global maximum in subfigures (a,b) and to the monomer concentration in subfigure (c).

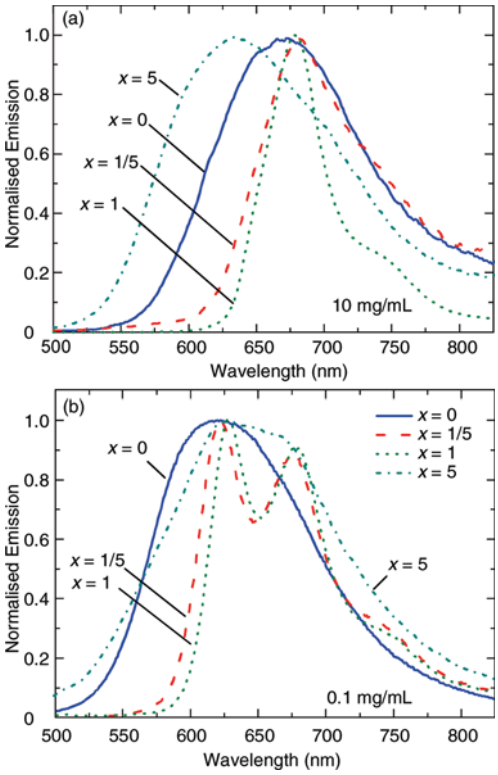

Figure 9. Normalized PL data of P3TMAHT−D_2O (solid blue curve) and P3TMAHT(SDS)$_x$−D_2O for x = 1/5 (dashed red curve), 1 (dotted green curve), and 5 (dashed and dotted cyan curve) at ~20 °C. The overall concentration was (a) ~10 or (b) ~0.1 mg/mL.

Table 4. Absorption (λ_{abs}) and Emission Maxima (λ_{em}) of P3TMAHT(SDS)$_x$ in D_2O[a]

x	overall concn (mg/mL)	λ_{abs} (nm)	λ_{em} (nm)
0	10.00	broad band, edge at 504	
0	~0.1	429	620, broad band
1/5	10.09	broad band, edge at 504	
1/5	~0.1	435, 507, 533 (sh), 579 (sh)	622, 675, structured band
1	10.28	546, 590	
1	~0.1	519 (sh), 559, 604	628, 679, structured band
5	10.46	420	
5	~0.1	422	626, 668 (sh), broad band with two components

[a] Excitation wavelength (λ_{ex}) was 430 nm. "sh" denotes shoulders.

twisted conformation along the polymer backbone. In fact, for x = 5, the emission maximum is considerably blue-shifted compared with the P3TMAHT−D_2O system, suggesting both the reduction in interchain interactions due to screening of polymer aggregates by SDS in this phase regime where SDS is present in (charge) excess, and also the improved solubilization of P3TMAHT into fully solubilized and separated chains.

Phase Diagram. The overall behavior of P3TMAHT(SDS)$_x$−D_2O can be understood at three levels: the equilibrium of polymer−surfactant aggregates and (possible) precipitate, the structure of aggregates as whole, and the polymer conformation inside (or absorbed onto) the aggregates.

Figure 10 plots a phenomenological phase diagram of aqueous P3TMAHT(SDS)$_x$ as a function of x at room temperature, when the overall concentration is ~1%. Also shown are schemes of the suggested main components (or aggregates) for each x, ranging from polymer aggregates (x = 0) to nearly pure SDS micelles (x > 5). Polymer−surfactant aggregates dominate for x = 1/5 to 5. Pure polymer aggregates and pure SDS micelles may also coexist with polymer−surfactant aggregates for $x \approx$ 1/5 and 5, respectively. As indicated by visual observation and the drop in optical density (Figure 8c), significant precipitation occurs only for x = 1.

Pure P3TMAHT (x = 0) forms charged aggregates containing several polymer chains that are ordered in a loose array in D_2O. For x = 1/5, P3TMAHT aggregates coexist with elongated (rod-like) P3TMAHT−SDS aggregates, which are associations of both P3TMAHT and SDS. This system does not show

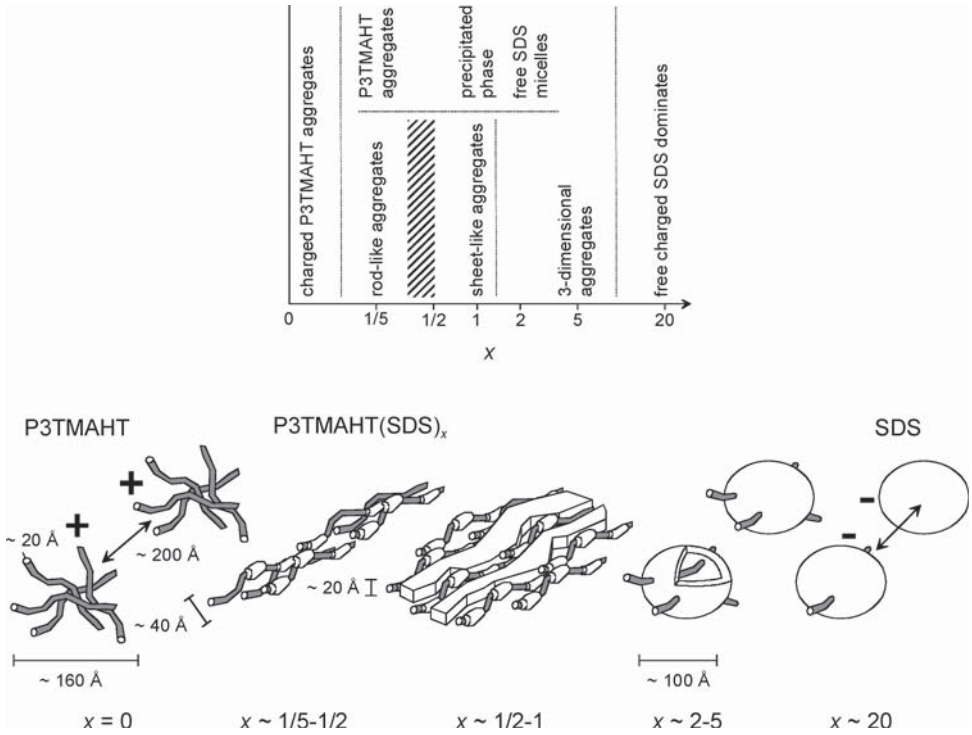

Figure 10. Top: Suggested phase diagram of P3TMAHT(SDS)$_x$−D_2O as a function of x at room temperature when the overall concentration is ∼1%. The dashed lines represent phenomenological phase transitions. Bottom: Schematic representations of the suggested aggregate structures in aqueous solutions. The gray and white areas refer to P3TMAHT and SDS, respectively.

long-range order, but the aggregates are randomly distributed in water. For x = 1/2 to 1, P3TMAHT(SDS)$_x$ forms sheet-like aggregates that coexist with emerging precipitation for x = 1. For x = 1/5 to 1/2, P3TMAHT appears as cylindrical multipolymer associations within these aggregates. For x = 1, these associations become sheet-like and most rigid. The transition from rod-like to sheet-like aggregates is not fully resolvable, but the data of P3TMAHT(SDS)$_{1/2}$ can be fitted to either the model of rod-like or sheet-like particles.

For x = 2−5, P3TMAHT(SDS)$_x$ forms ellipsoidal 3-D aggregates. As indicated by SAXS data, these aggregates appear essentially as SDS micelles. However, their charges are screened by polymer chains, which are either inside or absorbed onto them. For x = 20, the system characteristics are dominated by free SDS micelles that are ellipsoidal and charged showing long-range order in D_2O.

Conclusions

In summary, we have performed a systematic investigation of the phase behavior and structure formation of P3TMAHT(SDS)$_x$ in D_2O. At room temperature, the observed phase transitions are from charged P3TMAHT aggregates with interparticle order to rod-like (x = 1/5) and sheet-like particles (x = 1/2 to 1) with embedded polymer bundles (x = 1/5 to 1/2) or sheet-like (x = 1) polymer associations. Partial precipitation occurs at the charge compensation point (x = 1). Ellipsoidal particles, essentially SDS micelles modified by rod-like, dissolved polymer chains, occur beyond this point ($x \approx 5$). Polymer−SDS complexes for x = 1/5 to 5 show no interparticle order, whereas free SDS micelles dominate for x = 20. These transitions are followed by distinctive surfactochromic changes visibly observable as color transitions from pale red (P3TMAHT) to turbid violet (x = 1/5 to 1) and orange-yellow (x > 2). In the classical picture of McCullough, similar optical transitions for water-soluble PT polyelectrolytes are induced by steric factors with increasing counterion size. In the presented picture, the optical transitions are controlled by the increasing counterion fraction, where both steric factors and charge balance are changed. These transitions are explained in terms of increasingly complex structural reorganization. These results shed new light on the phase behavior of water-soluble π-conjugated polymers.

Acknowledgment. The SANS measurements were supported by the European Commission under the 7th Framework Programmes through the 'Research Infrastructures' action of the "Capacities Programme", contract No. CP-CSA_INFRA-2008-1.1.1 number 226507-NMI3. The SAXS measurements were supported by the European Community's 7th Framework Programme (FP7/2007-2013) under grant agreement No. 226716. R.C.E. thanks the Royal Irish Academy for financial support under the Mobility Grants scheme. Michael Forster of the University of Wuppertal is acknowledged for assistance and discussions.

Supporting Information Available: SANS data of SDS−D_2O, Holtzer plots of the SANS data of P3TMAHT(SDS-d_{25})$_x$−D_2O, the $p(r)$ functions calculated from the SANS data of P3TMAHT(SDS)$_x$−D_2O and P3TMAHT(SDS-d_{25})$_x$−D_2O, as well as excitation spectra of P3TMAHT(SDS)$_x$−D_2O.